

Search for Gamma-ray emission from Abell 119 galaxy cluster using INTEGRAL/ISGRI, COMPTEL, and DAMPE data.

Siddhant Manna^{1,*} and Shantanu Desai^{1,†}

¹ *Department of Physics, IIT Hyderabad Kandi, Telangana 502284, India*

We present a comprehensive search for non-thermal high-energy γ -ray emission from the nearby merging galaxy cluster Abell 119 ($z = 0.044$) using archival observations spanning over seven decades in photon energy. Our analysis combines hard X-ray data from INTEGRAL/ISGRI (30–100 keV), MeV γ -ray observations from COMPTEL (0.75–30 MeV), and GeV–TeV data from the DArk Matter Particle Explorer (DAMPE; 3 GeV–1 TeV). No statistically significant emission is detected at the cluster position in any energy band. In the hard X-ray regime, we derive a 3σ upper limit of $F_{30-100\text{ keV}} \lesssim 8.5 \times 10^{-11} \text{ erg cm}^{-2} \text{ s}^{-1}$ from ISGRI mosaic imaging. Reanalysis of archival COMPTEL data yields 95% confidence-level upper limits ranging from $\sim 9 \times 10^{-11}$ to $\sim 8 \times 10^{-10} \text{ erg cm}^{-2} \text{ s}^{-1}$ across 0.75–30 MeV. In the GeV–TeV range, DAMPE constrains the differential energy flux to $\sim 10^{-12}$ – $10^{-10} \text{ erg cm}^{-2} \text{ s}^{-1}$ (95% confidence level). These results provide independent multi-band constraints on the reported GeV excess from recent Fermi-LAT studies. While our DAMPE limits do not exclude the flux levels claimed in those analyses, the absence of confirmation across keV–MeV–GeV bands indicate that any non-thermal emission from Abell 119 remains tentative.

I. INTRODUCTION

Galaxy clusters are the most massive gravitationally bound structures in the Universe and can be used to probe cosmology [1–4] as well as fundamental physics [5–8]. Approximately 80% of the mass in these clusters is attributed to dark matter, while the intracluster medium (ICM) consisting of hot diffuse gas accounts for about 10–15% of their total mass [9, 10]. Although galaxy clusters have been mostly detected at all wavelengths from radio waves to X-rays, an unequivocal detection of gamma rays is still an open question. A summary of recent results in the searches for gamma-ray emission from individual galaxy clusters as well as stacked emission can be found in [11–15] and (references therein).

In one of our recent works [16], we carried out a systematic search for gamma-rays from 300 galaxy clusters selected from the 2500 sq. degree SPT-SZ survey [17, 18] based on their values M_{500}/z^2 using 15 years of Fermi-LAT data. From this search, we were able to detect a gamma-ray signature from one galaxy cluster (viz SPT-CL J2012-5649) with a significance of 6.1σ [16]. The signal was detected in the energy range between 1–10 GeV with a spectral index of approximately -3.6 . However, given the point spread function of Fermi-LAT, we could not ascertain if this signal is due to the intracluster medium or from radio galaxies in the vicinity of the cluster. This signal has been subsequently confirmed by other works [15]. We then searched for this signal in DArk Matter Particle Explorer (DAMPE) gamma-ray detector (between 3–1000 GeV) [19], COMPTEL (between 0.75–30 MeV) [20] and INTEGRAL/ISGRI (between 30–300 keV) [21]. However, null results were obtained for searches from all these detectors.

Another cluster for which tentative evidence for gamma-ray emission has recently been detected is Abell 119 [15, 22]. This cluster is a nearby massive galaxy cluster ($z = 0.044$) [23] with an estimated mass of $M \approx 3.05 \times 10^{14} M_{\odot}$ [24]. It is characterized by a high X-ray luminosity of approximately $3 \times 10^{44} \text{ erg s}^{-1}$, indicative of a dense and thermally energetic intracluster medium [25, 26]. Multiwavelength observations reveal that Abell 119 is dynamically disturbed, exhibiting evidence of past and possibly ongoing off-axis merger events [27]. In a dedicated study based on 14 years of observations, Harale and Paul [22] identified a $\sim 4\sigma$ excess of diffuse emission offset by $\sim 0.25^{\circ}$ from the cluster center, spatially overlapping with its virial region. Using spatially extended templates and various cosmic-ray proton (CRp) distribution models, they obtained Test Statistic (TS) values of ~ 18 , and derived integrated γ -ray fluxes in the 100 MeV–1 TeV band of $(10\text{--}12) \times 10^{-10} \text{ ph cm}^{-2} \text{ s}^{-1}$. The best-fit spectrum is characterized by a photon index of $\Gamma \approx 2.2$, corresponding to an inferred γ -ray luminosity of $\sim 1.2 \times 10^{43} \text{ erg s}^{-1}$. Interpreting the signal within a hadronic framework, they estimated a cosmic-ray proton-to-thermal energy fraction of $\sim 7\text{--}8\%$ and predicted an associated neutrino flux potentially detectable by next-generation observatories. However, the TS values remain below the canonical 5σ detection threshold (TS=25), and the authors cautioned that the signal does not yet constitute a firm detection. Around the same time, Li and Han [15] conducted a systematic search for γ -ray emission from 65 HIFLUGCS galaxy clusters

*Email:ph22resch11006@iith.ac.in

†Email:shntn05@gmail.com

using 16 years of Fermi-LAT data. Among these clusters Abell 119 exhibited a moderate excess with $TS \approx 20.7$ after optimized source localization, corresponding to an integrated flux of $(2.53 \pm 0.49) \times 10^{-10}$ ph cm $^{-2}$ s $^{-1}$ in the 0.5–500 GeV band. This significance remained below the formal detection threshold, and the authors noted the presence of radio sources in the nearby PMN catalog [28] within the 95% confidence region that could potentially contribute to the observed excess. For the clusters with $TS > 16$, dark matter annihilation scenarios were also found to be incompatible with constraints from dwarf spheroidal galaxies, favoring instead a hadronic cosmic-ray origin for the observed emission.

Prior searches for non-thermal emission from Abell 119 at hard X-ray energies have yielded only upper limits. A systematic analysis of HIFLUGCS galaxy clusters was conducted using joint data from the Swift/BAT all-sky survey data and XMM-Newton EPIC observations spanning 2–195 keV was done, searching for excess emission above the thermal intracluster medium component [29]. For Abell 119, their joint spectral fits produced a 90% confidence upper limit of 1.69×10^{-12} erg cm $^{-2}$ s $^{-1}$ on the 20–80 keV non-thermal flux (including systematic uncertainties). Assuming a fixed power-law index of $\Gamma = 2$, they derived a 3σ upper limit of 6.58×10^{-12} erg cm $^{-2}$ s $^{-1}$. Allowing the spectral index to vary yielded a best-fit value of $\Gamma \sim 2.12$ and a corresponding 3σ limit of 6.43×10^{-12} erg cm $^{-2}$ s $^{-1}$. These results indicate that there is no statistically significant excess at hard X-ray energies above the thermal emission from the cluster.

Despite these recent reported GeV excesses, the statistical significances remain below the formal 5σ detection threshold, and the origin of the emission remains uncertain. In particular, no confirmation has yet been obtained across independent instruments or complementary energy bands. While hard X-ray upper limits exist, no coordinated broadband analysis has tested the spectral consistency of the non-thermal interpretation from the keV to TeV regime for Abell 119. Such a multi-instrument study is required to assess the physical plausibility of the claimed excess and to place robust constraints on the cosmic-ray energy content of the cluster.

In this work, we search for high-energy emission from Abell 119 over a broad energy range spanning hard X-rays to TeV energies using archival observations from INTEGRAL/ISGRI, COMPTEL, and DAMPE. The structure of this manuscript is as follows. The data analysis procedures for each instrument are described in Sect. II. The results are presented in Sect. III. Finally, we summarize our findings in conclusions in Sect. IV.

II. DATA ANALYSIS

We perform a search for non-thermal emission from Abell 119 [22] using observations spanning keV to TeV energies. The analysis combines data from INTEGRAL/ISGRI [30, 31], COMPTEL [32], and DAMPE [33–35], providing energy coverage from ~ 30 keV to 1 TeV. Each instrument was analyzed independently using its standard data reduction and statistical framework. For instruments employing likelihood based analyses, the detection significance was quantified using the Test Statistic (TS), defined as

$$TS = -2 \ln \left(\frac{\mathcal{L}_0}{\mathcal{L}_1} \right), \quad (1)$$

where \mathcal{L}_0 and \mathcal{L}_1 denote the maximum likelihood values under the null (background-only) and source-included hypotheses, respectively. Under Wilks' theorem [36], TS asymptotically follows a half- χ^2 distribution with degrees of freedom equal to the number of additional free parameters in the source model [37]. One can then show that \sqrt{TS} approximates the detection significance in Gaussian standard deviations for one degree of freedom. In the absence of significant excess emission, 95% confidence-level flux upper limits were derived. The instrument-specific analysis procedures are described below.

A. INTEGRAL/ISGRI Data Analysis

The search for hard X-ray and soft γ -ray emission from Abell 119 was conducted using the ISGRI detector of the IBIS instrument [30] onboard INTEGRAL [31]. All publicly available Science Windows (ScWs) covering the position of Abell 119 (RA = 14.035°, Dec = -1.200° , J2000) were retrieved from the INTEGRAL Science Data Archive¹. After applying standard quality filters to exclude time intervals affected by solar flares and instrumental anomalies, a total of 38 Science windows were identified within a 5° radius of the cluster center (following the approach in [21]). All data were processed using the INTEGRAL Off-line Scientific Analysis software package (OSA v11.2) [38], following standard procedures outlined in the OSA User Manual² and consistent with our previous INTEGRAL analyses [21].

¹ <https://www.isdc.unige.ch/integral/archive>

² <https://www.astro.unige.ch/integral/analysis>

The image reconstruction was performed from the energy-corrected level (`startLevel = COR`) through the image reconstruction level (`endLevel = IMA2`). The default ISGRI reference catalog (`CAT_refCat = $ISDC_REF_CAT[ISGRI_FLAG>0]`) was adopted during processing. The imaging analysis was configured to produce sky mosaics in four logarithmically spaced energy bands: 30–41, 41–54.5, 54.5–73.5, and 73.5–99.5 keV, similar to our previous work [21]. These bands were chosen to optimize sensitivity given the energy-dependent effective area of ISGRI while maintaining adequate photon statistics. The lower bound of 30 keV reflects the degraded low-energy response of ISGRI after Revolution 1600 (mid-2015), as documented in the OSA User Manual [38], while the upper bound of ~ 100 keV avoids the rapidly declining effective area at higher energies.

Sky images were generated using the `ii_skyimage` task. Source detection employed a combined search approach (`OBS1_SearchMode = 3`) that includes catalog sources and up to 50 additional candidates, with a minimum detection significance threshold of 5σ for newly identified sources. The background subtraction was performed using the standard ISGRI background maps provided by the IBIS team. A mosaic image was constructed by combining all 38 ScWs with pixel spreading enabled (`OBS1_PixSpread = 1`) to improve the source localization accuracy.

The statistical significance at the source position was obtained directly from the ISGRI mosaic significance maps produced by `ii_skyimage`, which provide the significance in units of Gaussian standard deviations. We adopt a 5σ threshold (corresponding to a TS value of 25) as the criterion for a robust detection, consistent with standard practice in high-energy astrophysics [39].

B. COMPTEL Data Analysis

We now analyze archival COMPTEL observations to probe potential emission in the 0.75–30 MeV range, thereby bridging the gap between hard X-rays/soft gamma-rays and high-energy γ -rays.

The search for MeV γ -ray emission from Abell 119 was conducted using archival data from the Imaging Compton Telescope (COMPTEL) aboard the Compton Gamma Ray Observatory (CGRO), which operated from April 1991 through June 2000 [32]. COMPTEL was sensitive in the 0.75–30 MeV energy range with a field of view of approximately one steradian, achieving an energy resolution of 5–8% and an angular resolution of (1.7–4.4) $^\circ$ (FWHM), depending on energy [32]. To date, no subsequent mission has provided comparable all-sky imaging sensitivity in the MeV regime, making the COMPTEL archive uniquely valuable for studies of soft γ -ray emission from galaxy clusters. Recent developments in the GammaLib and ctools framework [40, 41] has facilitated the reanalysis of COMPTEL data. The data reduction and analysis procedures follow the methodologies detailed in our previous COMPTEL studies of galaxy clusters [20] and red dwarfs [42] which made use of these recent advancements, with adaptations specific to Abell 119. We summarize the key steps below.

We queried the COMPTEL archive to identify all viewing periods (VPs) that included Abell 119 within a 30° radius of the pointing direction, similar to [42], resulting in four suitable VPs. The `comobsselect` utility was used to extract the corresponding observations. To enable energy-resolved analysis, the `comobsbin` tool organized the data into logarithmically spaced energy bins spanning 0.75–30 MeV. Two binning configurations were employed: a fine scheme with 16 energy bins optimized for spectral characterization, following [20, 42], and a coarser 4-bin scheme designed to maximize photon statistics per bin, consistent with standard COMPTEL analysis practice³.

COMPTEL data are analyzed in a three-dimensional Compton data space defined by the reconstructed scatter angle ($\bar{\varphi}$) and two scatter direction coordinates (χ , ψ) [41]. Multiple viewing periods were merged using the `comobsadd` tool with the standard COMPTEL binning configuration: 80 bins with 1° spacing in each scatter direction coordinate and 25 bins with 2° spacing in scatter angle. The combined effective exposure from all four viewing periods totals 7.23×10^9 cm² s at the position of Abell 119. Model definition files were generated using `comobsmodel` for maximum-likelihood fitting. Abell 119 was modeled as a point source with a power-law spectrum characterized by normalization N_0 and photon index Γ . Standard COMPTEL instrumental background components were included in the likelihood model as implemented within GammaLib.

Spectral analysis was performed using the `csspec` tool. We adopted the BINS method, which replaces the assumed spectral model with independent normalization parameters in each energy bin, providing a model-independent approach particularly suitable for weak sources or non-detections. For each energy bin, the likelihood fit yields the flux estimate, statistical uncertainty, TS values, and 95% confidence upper limits. The detection significance was evaluated using TS defined in Eq. 1.

³ <http://cta.irap.omp.eu/ctools/users/tutorials/compTEL/index.html>

C. DAMPE Data Analysis

Next, we analyzed observations from the DAMPE, which provides sensitivity to γ rays between 3 GeV and 10 TeV [33–35]. The data reduction and analysis procedures closely follow the methodology detailed in our previous DAMPE study of the SPT-CL J2012-5649 cluster [19], with adaptations specific to Abell 119. We summarize the key steps below.

DAMPE achieves an angular resolution of $\leq 0.2^\circ$ at 100 GeV with a field of view of approximately 1.0 sr and provides an excellent energy resolution of $\sim 1\%$ at 100 GeV [34]. This advantage comes at the cost of a smaller acceptance, roughly seven times lower than that of Fermi-LAT. Detailed descriptions of the DAMPE detector subsystems and in-orbit performance calibrations can be found in Refs. [33–35].

We analyzed DAMPE photon data collected between January 1, 2016 and December 29, 2023, corresponding to the Mission Elapsed Time MET 94608000–346809600. The analysis was carried out using the DAMPE Science Tools (DmpST) software package [43], which combines photon event data, spacecraft pointing information, Monte Carlo instrument response functions (IRFs), and likelihood-based analysis tools. Photon events were selected within a circular region of interest (ROI) of radius 10° centered on the cluster position. The 10° ROI ensures adequate modeling of diffuse backgrounds while encompassing the instrument point-spread function at low energies, and is similar to that adopted in [19]. The energy range of the analysis was restricted to 3 GeV–1 TeV, where the DAMPE effective area, angular resolution, and background characterization are well understood. We retained only events satisfying the High-Energy Trigger (HET) selection criteria. Data recorded during passages through the South Atlantic Anomaly, periods affected by intense solar activity, and times when the target was more than 60° from the spacecraft Z -axis were excluded. The total livetime for the Abell 119 ROI is approximately 1.92×10^8 s.

Spatial binning was performed with a pixel size of 0.1° , while the energy range was divided into ten logarithmically spaced bins between 3 GeV and 1 TeV [19]. The source model consisted of a point-source component located at the cluster center, described by a power-law spectral model with spectral index initially fixed to $\Gamma = 2$, consistent with previous studies of galaxy clusters [11, 16]. Diffuse γ -ray backgrounds were modeled using the standard Galactic diffuse emission template `gll_iem_v07.fits` together with an isotropic component represented by a power-law spectral model. The normalizations of both diffuse components were treated as free parameters during the likelihood fitting procedure. A standard binned maximum-likelihood analysis was performed using the DmpST likelihood framework to determine the best-fit spectral parameters. The significance of the emission was quantified using TS, similar to the other detectors.

III. RESULTS

In the following subsections, we present the results of our multi-instrument search for non-thermal emission from Abell 119. No excess above 5σ was found in any of the analyzed energy bands, and we therefore obtain upper limits as presented in subsequent subsections.

A. INTEGRAL/ISGRI Hard X-ray Analysis

1. Source Detection and Catalog Cross-matching

The ISGRI mosaic images reveal multiple statistically significant point sources across the large field of view ($\sim 29^\circ \times 29^\circ$) [44]. Figure 1 presents the significance maps in all four energy bands. We identified a total of 28 sources within the analyzed region above the significance threshold of 5σ with 9 of those sources matching entries in the IBIS/ISGRI 1000-orbit source catalog [45] and 19 previously uncatalogued sources (marked with green circles in Figure 1). The newly detected sources likely correspond to previously uncatalogued hard X-ray emitters; detailed identification is beyond the scope of this work.

2. Search for Emission from Abell 119

To assess potential association between detected sources and Abell 119, we computed the angular separation of all sources from the cluster center (RA = 14.035° , Dec = -1.200° , J2000). Table I lists all detected sources sorted by angular distance from the cluster. Critically, the nearest detected source lies at an angular separation of $\sim 290'$ ($\sim 4.8^\circ$), far beyond both the ISGRI point spread function (PSF; FWHM $\sim 12'$) [30, 31]. None of the 28 detected sources show spatial coincidence with the cluster.

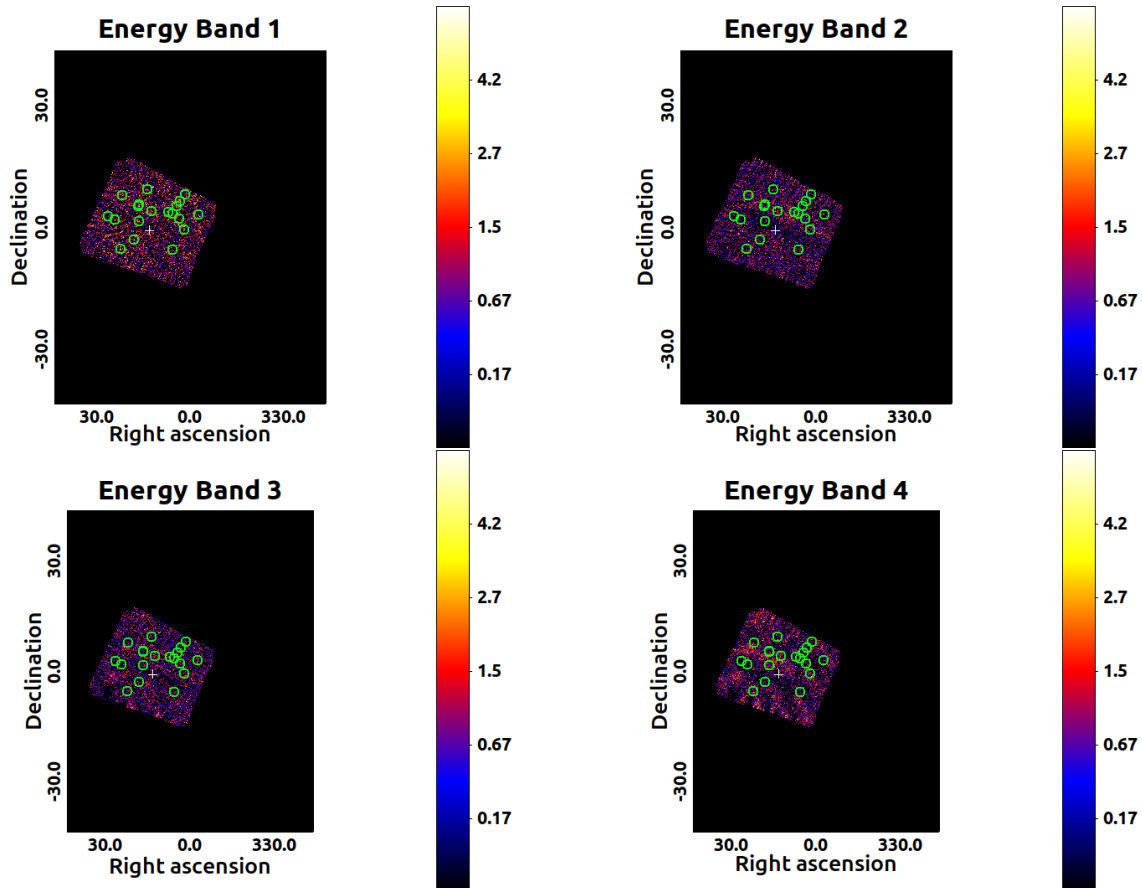


FIG. 1: INTEGRAL/ISGRI mosaic significance maps of the Abell 119 field in four logarithmically spaced energy bands: Band 1 (30–41 keV; *top left*), Band 2 (41–54.5 keV; *top right*), Band 3 (54.5–73.5 keV; *bottom left*), and Band 4 (73.5–99.5 keV; *bottom right*). The white cross marks the cluster center at RA = 14.035°, Dec = -1.200° (J2000). Green circles indicate sources detected at $> 5\sigma$ significance in the ISGRI mosaic images. The color scale ranges from 0σ (blue) to $+6\sigma$ (red). No significant emission is detected at the position of Abell 119 in any energy band.

We quantified the detection significance at the exact position of Abell 119 by extracting values from the mosaic significance maps in each energy band. We found the maximum TS value to be 1.1 in 30–41 keV energy band. Table II presents these results. In all the four energy bands, the significance at the cluster center remains well below the canonical 5σ detection threshold, with values ranging from $(0-1.2)\sigma$. These measurements are fully consistent with background fluctuations and provide no evidence for hard X-ray or soft γ -ray emission associated with the cluster. Based on these null detections, we derive 3σ upper limits on the hard X-ray flux from Abell 119, as detailed below.

3. Flux Upper Limits

Given the non-detection of Abell 119 in all the ISGRI energy bands, we derive conservative flux upper limits using a purely image-based approach that avoids the systematic uncertainties associated with spectral fitting of coded-mask telescope data, as done in [21, 46]. We focus on the combined 30–100 keV band to maximize photon statistics while remaining within the optimal energy range of ISGRI, before the rapid decline of effective area above ~ 100 keV.

The statistical uncertainty at the cluster position was extracted directly from the mosaic variance map, which encodes the photon counting statistics and systematic uncertainties from the imaging reconstruction. The 1σ count-rate uncertainty is given by

$$\sigma_{\text{cnt}} = \sqrt{V}, \quad (2)$$

where V is the variance value at the pixel corresponding to the cluster coordinates. For Abell 119, we obtain

$$\sigma_{\text{cnt}} = 0.193 \text{ counts s}^{-1}. \quad (3)$$

TABLE I: ISGRI sources detected within the Abell 119 field, sorted by angular separation from the cluster center (RA = 14.035°, Dec = −1.200°, J2000). The table lists both cataloged sources [45] and new detections from this work. All sources lie well outside the ISGRI PSF (FWHM $\sim 12'$) [30].

Source Name	Type	RA (deg)	Dec (deg)	Separation (arcmin)
NEW_11	New	17.5343	2.1175	289.3
NEW_13	New	19.1219	−3.9904	347.8
NEW_7	New	13.2397	5.6958	416.5
NEW_10	New	7.6001	5.4461	554.7
NEW_12	New	17.7180	7.1789	549.0
NEW_17	New	17.5749	7.5801	567.8
NEW_8	New	6.0631	−7.9744	626.3
NEW_3	New	3.9155	2.9055	655.1
NEW_15	New	23.1003	−7.0785	646.9
NEW_19	New	24.8955	2.4303	686.9
NEW_1	New	2.1170	−0.8284	715.3
NEW_6	New	4.7785	7.3055	753.3
NEW_4	New	26.7931	3.6057	817.6
NEW_9	New	14.6750	12.7249	836.4
NEW_16	New	22.7021	10.2784	861.5
NEW_2	New	3.3959	9.0909	886.4
NEW_18	New	1.6561	11.4312	1058.0
NEW_5	New	356.8664	4.3916	1082.6
Mrk 1152	Catalog	18.4587	−14.8456	859.7
IGR J01528−0326	Catalog	28.2042	−3.4468	860.0
IGR J01528−0845	Catalog	28.2340	−8.7690	962.0
Mrk 584	Catalog	30.0990	2.7110	991.7
NGC 788	Catalog	30.2769	−6.8155	1028.5
Mrk 1018	Catalog	31.5667	−0.2914	1053.2
IGR J23558−1047	Catalog	358.9951	−10.7791	1064.8
NGC 7603	Catalog	349.7359	0.2435	1460.4
PKS 2325+093	Catalog	351.9370	9.6660	1472.4

TABLE II: Detection significance at the Abell 119 cluster center extracted from ISGRI mosaic significance maps. All values are consistent with background fluctuations.

Energy Range (keV)	Significance (σ)
30–41	1.21
41–54.5	0.00
54.5–73.5	0.40
73.5–99.5	0.00

Adopting a conservative 3σ confidence level appropriate for upper limit determinations in non-detections, the count rate is

$$C_{3\sigma} = 3\sigma_{\text{cnt}} = 0.579 \text{ counts s}^{-1}. \quad (4)$$

To convert this count-rate upper limit into a physical energy flux, we employ an empirical calibration based on contemporaneous ISGRI observations of the Crab Nebula, processed through an identical analysis pipeline with matching energy bands and mosaic parameters [21, 46]. This approach accounts for the energy-dependent instrumental response, effective area, and imaging systematics. We assume the standard Crab spectrum in the hard X-ray band [46]:

$$N(E) = 10 E^{-2.1} \text{ ph cm}^{-2} \text{ s}^{-1} \text{ keV}^{-1}, \quad (5)$$

and compute the integrated energy flux in the 30–100 keV band along with the corresponding ISGRI count rate. The resulting calibration factor is then applied to our measured upper limit.

This procedure yields a 3σ upper limit on the energy flux from Abell 119 of

$$F_{3\sigma}(30\text{--}100 \text{ keV}) = 8.5 \times 10^{-11} \text{ erg cm}^{-2} \text{ s}^{-1}. \quad (6)$$

For comparison with previous INTEGRAL studies of galaxy clusters and other faint hard X-ray sources, this limit corresponds to approximately 8–10 mCrab, where 1 mCrab $\sim (0.8\text{--}1.0) \times 10^{-11} \text{ erg cm}^{-2} \text{ s}^{-1}$ in

the 20–100 keV range [45]. This constraint represents one of the most stringent limits on soft γ -ray emission from Abell 119 achieved with INTEGRAL/ISGR1 to date. The model-independent, image-based methodology employed here avoids potential systematic biases from spectral fitting procedures and source confusion that can affect coded-mask telescope analyses in crowded fields.

B. COMPTEL MeV Gamma-Ray Analysis

1. Maximum-Likelihood Spectral Analysis

We performed two independent likelihood analyses with complementary energy binning strategies to test for potential emission while maximizing statistical robustness. An initial fit over the full 0.75–30 MeV range using 16 logarithmically spaced energy bins treated both N_0 and Γ as free parameters, with the source position and E_0 held fixed. This configuration yielded $TS = 0.61$, far below the detection threshold ($TS > 25$ for 5σ significance). The best-fit normalization was consistent with zero within uncertainties, and the background model alone adequately reproduced the observed photon distribution across all energy bins.

To improve statistical stability and reduce sensitivity to energy-dependent systematic effects, we repeated the analysis using four broader energy bins corresponding to COMPTEL’s native energy bands (see Table III). An unconstrained fit with both spectral parameters free again produced $TS \approx 0$. We then performed a constrained fit fixing the photon index at $\Gamma = 2.0$, a value characteristic of hadronic γ -ray emission from cosmic-ray interactions [47]. This analysis converged with $TS \approx 0$ and showed excellent agreement between the model-predicted event count and the observed count, confirming that the background-only hypothesis provides a statistically adequate description of the data. Both analyses consistently indicate no statistically significant MeV γ -ray emission from Abell 119.

2. Energy-Resolved Upper Limits

Following the null detection in the likelihood analysis, we derived 95% confidence-level upper limits in each of four logarithmically spaced energy bins spanning 0.75–30 MeV. Table III summarizes the results. All energy bins yield $TS \lesssim 2$, confirming the absence of detectable emission. The 95% upper limits on the integrated energy flux range from $\sim 9 \times 10^{-11}$ to $\sim 8 \times 10^{-10}$ erg cm $^{-2}$ s $^{-1}$, with the most stringent constraints obtained in the 0.75–1.89 MeV band. Figure 2 presents the Spectral Energy Distribution (SED) plot showing upper limits across the full MeV range.

TABLE III: Energy-resolved 95% confidence upper limits on MeV γ -ray flux from Abell 119 derived from COMPTEL observations. The TS values in all bins are consistent with background fluctuations ($TS \lesssim 2$), indicating no significant detection.

Energy Range (MeV)	Flux Upper Limit (erg cm $^{-2}$ s $^{-1}$)	TS
0.75 – 1.89	$< 8.87 \times 10^{-11}$	0.01
1.89 – 4.74	$< 3.56 \times 10^{-10}$	0.02
4.74 – 11.93	$< 8.14 \times 10^{-10}$	1.97
11.93 – 30.00	$< 6.67 \times 10^{-10}$	0.01

C. DAMPE GeV–TeV Gamma-Ray Analysis

1. Broadband Likelihood Analysis

The broadband fit models potential emission from Abell 119 as a point source centered at the cluster coordinates (RA = 14.035°, Dec = −1.200°, J2000) with a power-law spectrum. No statistically significant emission is detected from the cluster position. The best-fit Test Statistic is $TS \simeq 0$, indicating that the inclusion of a source at the Abell 119 location does not improve the likelihood relative to the background-only hypothesis. This result is fully consistent with statistical fluctuations. As expected for a non-detection, the fitted photon spectral index is poorly constrained. The diffuse background components dominate the photon counts within the ROI.

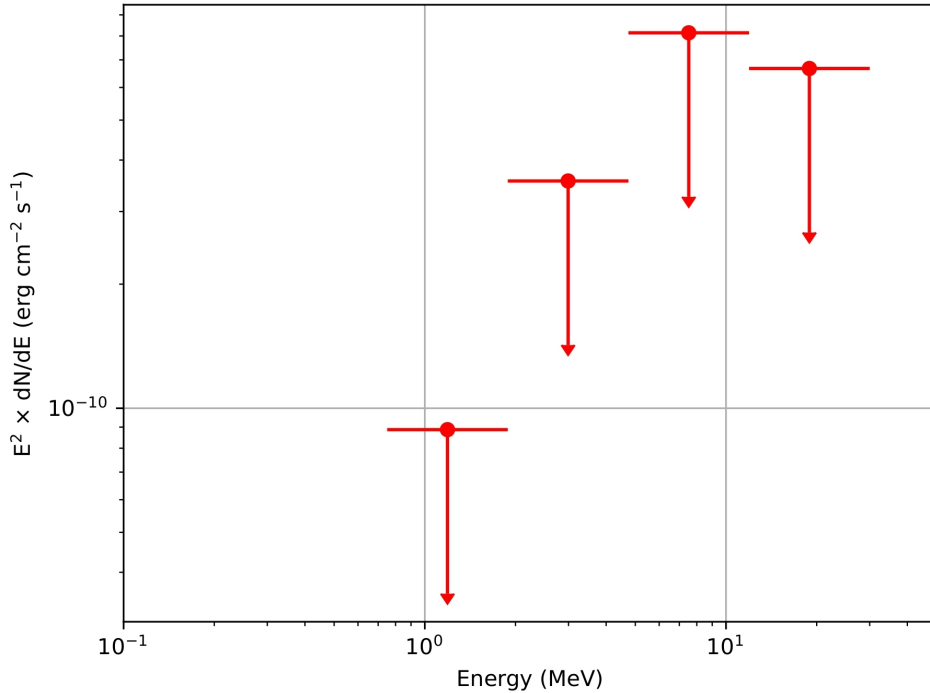


FIG. 2: SED plot of Abell 119 in the MeV band from COMPTEL observations. The data points represent 95% confidence-level upper limits on $E^2 dN/dE$ derived from bin-by-bin maximum-likelihood analysis in four logarithmically spaced energy bins covering 0.75–30 MeV. No statistically significant γ -ray emission is detected.

2. Energy-Resolved Analysis and Upper Limits

To investigate possible energy-dependent features, we performed a bin-by-bin likelihood analysis using ten logarithmically spaced energy bins spanning 3 GeV to 1 TeV, as also done in [19]. In each bin, the source normalization was treated as a free parameter while fixing the photon index to $\Gamma = 2.0$.

In all DAMPE energy bins, the TS values remain far below the canonical detection threshold of $TS = 25$, indicating the absence of any statistically significant γ -ray emission from Abell 119. We therefore derive bin-by-bin 95% confidence-level upper limits on the energy flux across the full DAMPE energy range. The resulting SED plot is shown in Figure 3, where the upper limits span nearly two orders of magnitude, from $\sim 10^{-12}$ to $\sim 10^{-10}$ $\text{erg cm}^{-2} \text{s}^{-1}$ between 3 GeV and 1 TeV. The numerical values of the upper limits, together with the corresponding TS values, are reported in Table IV. The absence of significant emission across the entire 3 GeV–1 TeV band implies that any GeV–TeV γ -ray emission from Abell 119 must lie below the current sensitivity of DAMPE.

TABLE IV: Energy-resolved 95% confidence upper limits on GeV–TeV γ -ray flux from Abell 119 derived from DAMPE observations. The TS values in all bins remain well below the detection threshold ($TS < 25$), indicating no significant emission.

Energy Range (GeV)	Flux Upper limits ($\text{erg cm}^{-2} \text{s}^{-1}$)	TS
3.0 – 5.4	$< 1.5 \times 10^{-12}$	0.15
5.4 – 9.6	$< 1.6 \times 10^{-12}$	0.06
9.6 – 17.1	$< 2.9 \times 10^{-12}$	0.02
17.1 – 30.6	$< 4.6 \times 10^{-12}$	0.01
30.6 – 54.8	$< 1.8 \times 10^{-11}$	0.30
54.8 – 97.9	$< 3.5 \times 10^{-11}$	0.07
97.9 – 175.0	$< 3.7 \times 10^{-11}$	0.11
175.0 – 312.9	$< 7.7 \times 10^{-11}$	0.03
312.9 – 559.4	$< 1.6 \times 10^{-10}$	0.01
559.4 – 1000	$< 3.5 \times 10^{-10}$	0.02

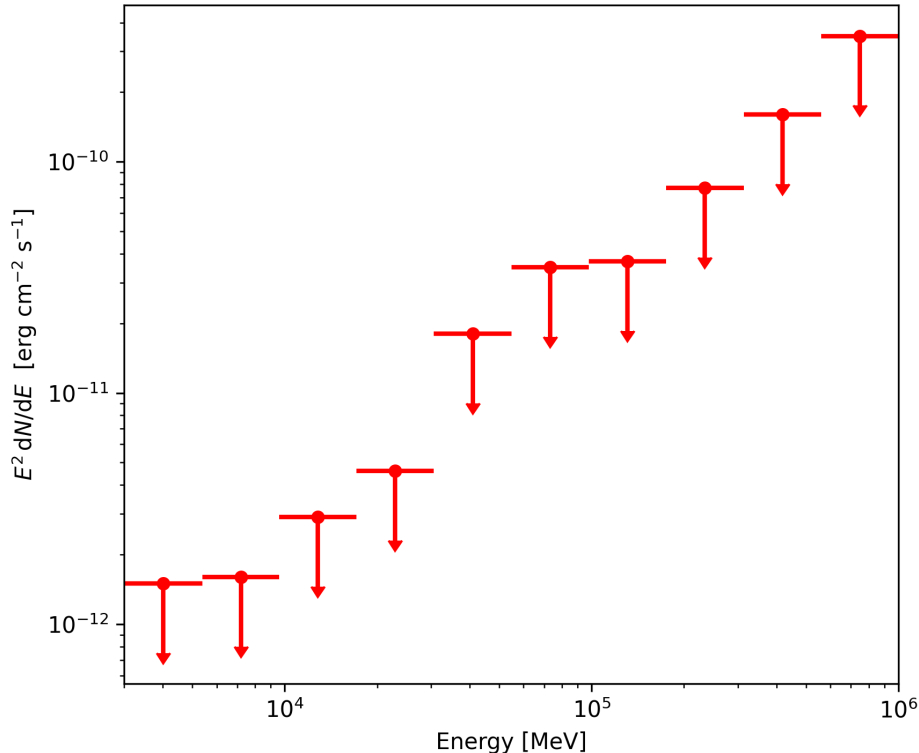


FIG. 3: SED plot of Abell 119 from DAMPE observations. The data points represent 95% confidence-level upper limits on $E^2 dN/dE$ derived from bin-by-bin likelihood analysis in ten logarithmically spaced energy bins between 3 GeV and 1 TeV. No significant γ -ray excess is detected in any energy bin.

D. Combined Analysis

To enable a uniform comparison of non-thermal constraints across multiple instruments and energy ranges, we performed a combined analysis of Abell 119 spanning hard X-rays to TeV energies, incorporating archival observations from Swift/BAT, INTEGRAL/ISGRI, COMPTEL, DAMPE, and Fermi-LAT. For energy-binned instruments (Swift/BAT, INTEGRAL/ISGRI, COMPTEL, and DAMPE), fluxes are plotted at the geometric mean energy of each bin, with downward arrows denoting upper limits.

For Swift/BAT and INTEGRAL/ISGRI, we adopted published 3σ upper limits on non-thermal emission in the 20–80 keV and 30–100 keV bands, respectively. COMPTEL upper limits were derived using the `csspec` framework within `ctools`, as shown in Table III and DAMPE upper limits were obtained from energy-resolved likelihood analyses as depicted in Table IV. For the Fermi-LAT measurement, we adopted the spatial model yielding the maximum TS (TS = 18.47; galaxy-density template) [22]. The associated band-integrated photon flux in the 100 MeV–1 TeV range was converted to an energy flux assuming a power-law spectrum with photon index $\Gamma \approx 2.2$, and plotted at the geometric mean energy of the band. Figure 4 presents the resulting SED of Abell 119, spanning over seven decades in energy. This combined representation enables a direct visual and quantitative assessment of the compatibility between the tentative GeV excess reported by Harale and Paul [22] and the non-thermal upper limits derived from hard X-ray and MeV–TeV observations.

IV. CONCLUSIONS

We have carried out a comprehensive broadband search for non-thermal high-energy emission from Abell 119 using archival observations from INTEGRAL/ISGRI (30–100 keV), COMPTEL (0.75–30 MeV), and DAMPE (3 GeV–1 TeV), providing coverage from hard X-rays to TeV γ -rays.

In the hard X-ray band, INTEGRAL/ISGRI reveals no statistically significant emission in any of the energy bands (30–41, 41–54.5, 54.5–73.5, and 73.5–99.5 keV), with all significances below 1.5σ . We derive a 3σ upper limit on the integrated 30–100 keV flux of

$$F_{30-100 \text{ keV}} \lesssim 8.5 \times 10^{-11} \text{ erg cm}^{-2} \text{ s}^{-1},$$

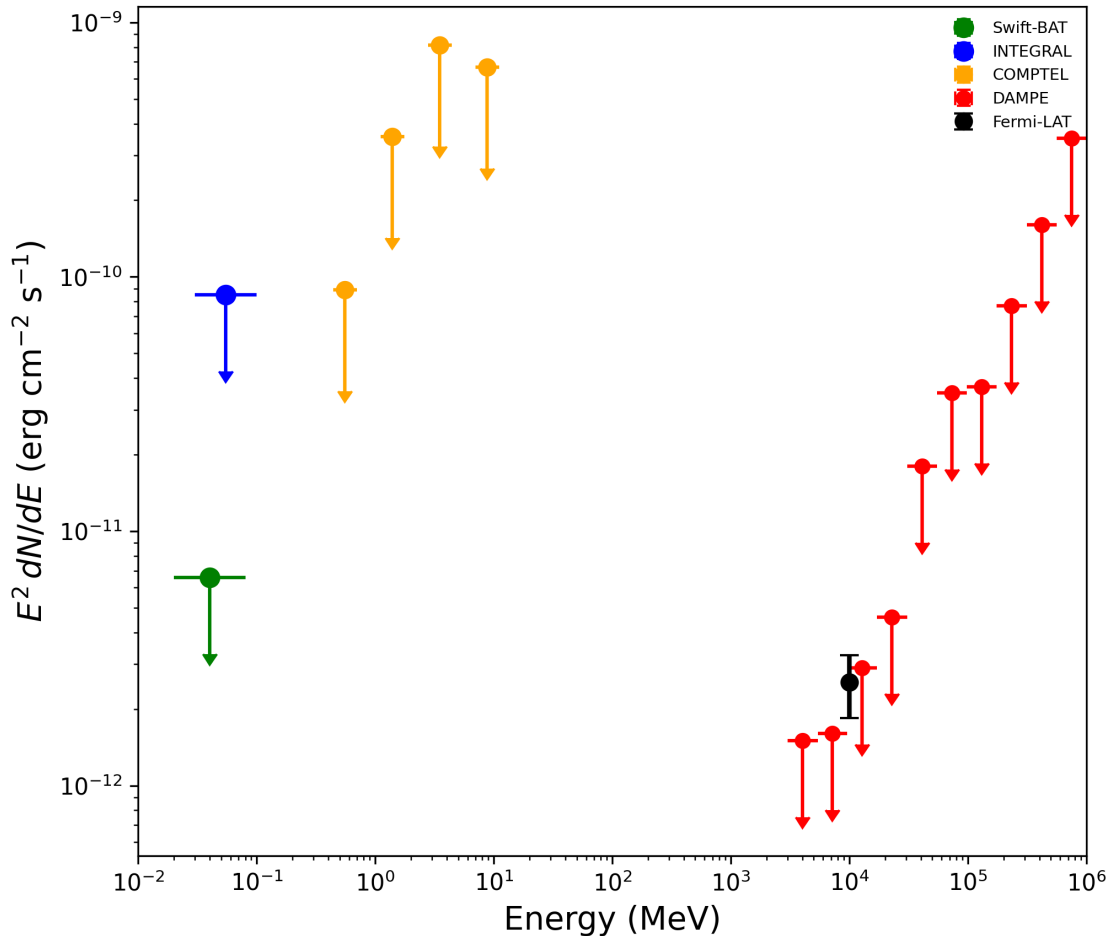


FIG. 4: SED plot of Abell 119 from hard X-rays to GeV energies. Downward arrows with horizontal energy bars denote upper limits from Swift/BAT, INTEGRAL/ISGRI, COMPTEL, and DAMPE. The Fermi-LAT point shows the band-integrated energy flux for the maximum-TS spatial model of Harale and Paul [22].

consistent with, though less stringent than, the 90% confidence limit of $1.69 \times 10^{-12} \text{ erg cm}^{-2} \text{ s}^{-1}$ (20–80 keV) from the joint Swift/BAT and XMM-Newton analysis [29]. Both studies independently exclude any significant hard X-ray excess above thermal intracluster emission, placing stringent constraints on inverse Compton or synchrotron emission from relativistic electrons in the cluster.

COMPTEL reanalysis yields no significant excess in broadband or energy-resolved fits (TS < 25 throughout), with 95% confidence upper limits ranging from $\sim 9 \times 10^{-11} \text{ erg cm}^{-2} \text{ s}^{-1}$ at 0.75–1.89 MeV to $\sim 8 \times 10^{-10} \text{ erg cm}^{-2} \text{ s}^{-1}$ at higher energies, representing the first COMPTEL constraints on soft γ -ray emission from this cluster. Similarly, the DAMPE likelihood analysis finds no significant GeV–TeV emission (broadband TS ~ 0), with 95% confidence upper limits of $\sim 10^{-12}$ – $10^{-10} \text{ erg cm}^{-2} \text{ s}^{-1}$ across 3 GeV–1 TeV.

In comparison, recent Fermi-LAT analyses report GeV signals with marginal significance ($4 - 4.5\sigma$), having integrated photon fluxes $\sim 10^{-9} \text{ ph cm}^{-2} \text{ s}^{-1}$ [15, 22]. The latter work also identified several PMN radio sources [28] within the 95% localization region of the excess, suggesting possible point-source contamination. Our DAMPE upper limits which are in the energy range from ~ 3 – 10 GeV range do not independently rule out the claimed detections, but confirm that any emission lies near the sensitivity floor of current instruments.

To report these constraints in a holistic fashion, we constructed a combined SED of Abell 119 spanning over seven decades in energy, incorporating upper limits from Swift/BAT, INTEGRAL/ISGRI, COMPTEL, and DAMPE alongside the Fermi-LAT measurement of Harale and Paul [22]. This representation enables a direct visual and quantitative comparison between the tentative GeV excess and the non-thermal constraints at lower and higher energies, clearly illustrating that any non-thermal component in Abell 119 must lie well below current instrumental sensitivities across the full keV–TeV band.

Definitive conclusions await next-generation MeV observatories such as COSI, AMEGO-X as well as improved GeV–TeV facilities (such as CTA), which will be essential to determine whether genuine non-thermal emission is present in Abell 119.

ACKNOWLEDGEMENTS

SM thanks the Ministry of Education (MoE), Government of India, for financial support through a research fellowship that enabled this work. This research is based on observations with INTEGRAL, an ESA project with instruments and a Science Data Centre funded by ESA Member States (particularly the PI countries: Denmark, France, Germany, Italy, Switzerland, and Spain), as well as the Czech Republic and Poland, with the participation of Russia and the USA. We acknowledge the use of public data from the INTEGRAL Science Data Centre (ISDC).

This work also uses archival COMPTEL data obtained from the Compton Gamma Ray Observatory (CGRO) mission archive. We also acknowledge the use of data from the Dark Matter Particle Explorer (DAMPE) mission, supported by the Strategic Priority Program on Space Science, and the data services provided by the National Space Science Data Center of China.

-
- [1] S. D. M. White and M. J. Rees, *MNRAS* **183**, 341 (1978).
 - [2] A. V. Kravtsov and S. Borgani, *Ann. Rev. Astron. Astrophys.* **50**, 353 (2012), 1205.5556.
 - [3] S. W. Allen, A. E. Evrard, and A. B. Mantz, *Ann. Rev. Astron. Astrophys.* **49**, 409 (2011), 1103.4829.
 - [4] A. A. Vikhlinin, A. V. Kravtsov, M. L. Markevich, R. A. Sunyaev, and E. M. Churazov, *Physics Uspekhi* **57**, 317-341 (2014).
 - [5] S. Desai, *Physics Letters B* **778**, 325 (2018), 1708.06502.
 - [6] K. Bora and S. Desai, *JCAP* **2021**, 012 (2021), 2008.10541.
 - [7] K. Bora and S. Desai, *JCAP* **2021**, 052 (2021), 2104.00974.
 - [8] K. Bora, R. F. L. Holanda, S. Desai, and S. H. Pereira, *European Physical Journal C* **82**, 17 (2022), 2106.15805.
 - [9] K. Murase and J. F. Beacom, *JCAP* **2013**, 028 (2013), 1209.0225.
 - [10] A. Condorelli, J. Biteau, and R. Adam, *Astrophys. J.* **957**, 80 (2023), 2309.04380.
 - [11] V. Baghmany, D. Zargaryan, F. Aharonian, R. Yang, S. Casanova, and J. Mackey, *MNRAS* **516**, 562 (2022), 2110.00309.
 - [12] U. Keshet, *JCAP* **2025**, 016 (2025), 2502.19494.
 - [13] S. Manna and S. Desai, *Physics of the Dark Universe* **49**, 101966 (2025), 2502.15235.
 - [14] J. Pérez-Romero, M. di Mauro, R. Adam, M. Á. Sánchez-Conde, and G. Zaharijas, *arXiv e-prints arXiv:2509.15720* (2025), 2509.15720.
 - [15] S. Li and F. Han, *Astrophys. J.* **997**, 227 (2026).
 - [16] S. Manna and S. Desai, *JCAP* **2024**, 017 (2024), 2310.07519.
 - [17] L. E. Bleem, B. Stalder, T. de Haan, K. A. Aird, S. W. Allen, D. E. Applegate, M. L. N. Ashby, M. Bautz, M. Bayliss, B. A. Benson, et al., *Astrophys. J. Suppl. Ser.* **216**, 27 (2015), 1409.0850.
 - [18] S. Bocquet, J. P. Dietrich, T. Schrabback, L. E. Bleem, M. Klein, S. W. Allen, D. E. Applegate, M. L. N. Ashby, M. Bautz, M. Bayliss, et al., *Astrophys. J.* **878**, 55 (2019), 1812.01679.
 - [19] S. Manna and S. Desai, *Journal of High Energy Astrophysics* **44**, 210 (2024), 2408.10983.
 - [20] S. Manna and S. Desai, *JCAP* **2024**, 013 (2024), 2401.13240.
 - [21] S. Manna, S. Desai, and R. A. Krivonos, *arXiv e-prints arXiv:2512.12616* (2025), 2512.12616.
 - [22] G. D. Harale and S. Paul, *Phys. Rev. D* **112**, 103025 (2025), 2511.15559.
 - [23] R. J. Smith, M. J. Hudson, J. E. Nelan, S. A. W. Moore, S. J. Quinney, G. A. Wegner, J. R. Lucey, R. L. Davies, J. J. Malecki, D. Schade, et al., *The Astronomical Journal* **128**, 1558 (2004).
 - [24] M. J. Way, H. Quintana, and L. Infante, *arXiv e-prints astro-ph/9709036* (1997), astro-ph/9709036.
 - [25] Y. Lee, S.-C. Rey, M. Hilker, Y.-K. Sheen, and S. K. Yi, *Astrophys. J.* **822**, 92 (2016), 1603.01556.
 - [26] M. Markevitch, W. R. Forman, C. L. Sarazin, and A. Vikhlinin, *Astrophys. J.* **503**, 77 (1998), astro-ph/9711289.
 - [27] C. B. Watson, E. L. Blanton, S. W. Randall, C. L. Sarazin, A. Sarkar, J. A. ZuHone, and E. M. Douglass, *Astrophys. J.* **955**, 103 (2023), 2308.04367.
 - [28] A. E. Wright, M. R. Griffith, B. F. Burke, and R. D. Ekers, *Astrophys. J. Suppl. Ser.* **91**, 111 (1994).
 - [29] D. R. Wik, C. L. Sarazin, Y.-Y. Zhang, W. H. Baumgartner, R. F. Mushotzky, J. Tueller, T. Okajima, and T. E. Clarke, *Astrophys. J.* **748**, 67 (2012), 1207.0506.
 - [30] P. Ubertini, F. Lebrun, G. Di Cocco, A. Bazzano, A. J. Bird, K. Broenstad, A. Goldwurm, G. La Rosa, C. Labanti, P. Laurent, et al., *Astron. & Astrophys.* **411**, L131 (2003).
 - [31] C. Winkler, T. J.-L. Courvoisier, G. Di Cocco, N. Gehrels, A. Giménez, S. Grebenev, W. Hermsen, J. M. Mas-Hesse, F. Lebrun, N. Lund, et al., *Astron. & Astrophys.* **411**, L1 (2003).
 - [32] V. Schoenfelder, H. Aarts, K. Bennett, H. de Boer, J. Clear, W. Collmar, A. Connors, A. Deerenberg, R. Diehl, A. von Dordrecht, et al., *Astrophys. J. Suppl. Ser.* **86**, 657 (1993).
 - [33] J. Chang, *Chinese Journal of Space Science* **34**, 550 (2014).
 - [34] J. Chang, G. Ambrosi, Q. An, R. Asfandiyarov, P. Azzarello, P. Bernardini, B. Bertucci, M. S. Cai, M. Caragiulo, D. Y. Chen, et al., *Astroparticle Physics* **95**, 6 (2017), 1706.08453.
 - [35] G. Ambrosi, Q. An, R. Asfandiyarov, P. Azzarello, P. Bernardini, M. S. Cai, M. Caragiulo, J. Chang, D. Y. Chen, H. F. Chen, et al., *Astroparticle Physics* **106**, 18 (2019), 1907.02173.
 - [36] S. S. Wilks, *Annals Math. Statist.* **9**, 60 (1938).

- [37] J. R. Mattox, D. L. Bertsch, J. Chiang, B. L. Dingus, S. W. Digel, J. A. Esposito, J. M. Fierro, R. C. Hartman, S. D. Hunter, G. Kanbach, et al., *Astrophys. J.* **461**, 396 (1996).
- [38] T. J.-L. Courvoisier, R. Walter, V. Beckmann, A. J. Dean, P. Dubath, R. Hudec, P. Kretschmar, S. Mereghetti, T. Montmerle, N. Mowlavi, et al., *Astron. & Astrophys.* **411**, L53 (2003), astro-ph/0308047.
- [39] L. Lyons, arXiv e-prints arXiv:1310.1284 (2013), 1310.1284.
- [40] J. Knödseder, M. Mayer, C. Deil, J. B. Cayrou, E. Owen, N. Kelley-Hoskins, C. C. Lu, R. Buehler, F. Forest, T. Louge, et al., *Astron. & Astrophys.* **593**, A1 (2016), 1606.00393.
- [41] J. Knödseder, W. Collmar, M. Jarry, and M. McConnell, *Astron. & Astrophys.* **665**, A84 (2022), 2207.13404.
- [42] N. Shrivastava, S. Manna, and S. Desai, *JCAP* **2024**, 029 (2024), 2407.01060.
- [43] K.-K. Duan, W. Jiang, Y.-F. Liang, Z.-Q. Shen, Z.-L. Xu, Y.-Z. Fan, F. Gargano, S. Garrappa, D.-Y. Guo, S.-J. Lei, et al., *Research in Astronomy and Astrophysics* **19**, 132 (2019), 1904.13098.
- [44] F. Lebrun, J. P. Leray, P. Lavocat, J. Créton, M. Arquès, C. Blondel, C. Bonnin, A. Bouère, C. Cara, T. Chaleil, et al., *Astron. & Astrophys.* **411**, L141 (2003), astro-ph/0310362.
- [45] A. J. Bird, A. Bazzano, A. Malizia, M. Flocchi, V. Sguera, L. Bassani, A. B. Hill, P. Ubertini, and C. Winkler, *Astrophys. J. Suppl. Ser.* **223**, 15 (2016), 1601.06074.
- [46] R. Krivonos, S. Tsygankov, M. Revnivtsev, S. Grebenev, E. Churazov, and R. Sunyaev, *Astron. & Astrophys.* **523**, A61 (2010), 1006.4437.
- [47] M. Ackermann, M. Ajello, A. Albert, A. Allafort, W. B. Atwood, L. Baldini, J. Ballet, G. Barbiellini, D. Bastieri, K. Bechtol, et al., *Astrophys. J.* **787**, 18 (2014), 1308.5654.